Compact Tunable Bandpass Filter With a Fixed Out-of-Band Rejection Based on Hilbert Fractals

Hong-Li Peng, *Member, IEEE*, Lin-Sheng Wu, *Member, IEEE*, Wen-Yan Yin, *Senior Member, IEEE*, David Huo, *Member, IEEE*, and Junfa Mao, *Fellow, IEEE*

***Abstract*— This paper proposes a new type of compact tunable bandpass filter with bandwidth tuning and out-of-band fixed rejection. Because we employ the modified Hilbert fractal structure loaded with varactors as resonators, the tunable filter has a very compact configuration and a constant shape over the entire tuning range. The frequency selectivity is improved by introducing a cross coupling between the source and the load. As a result of the utilization of a pair of properly designed feedlines, the frequency tuning and the out-of-band rejection of the filter are independent of each other, which simplifies its operation significantly. Two filter prototypes have been realized with the same size of 25.0 × 17.0 × 1.0 mm^3. Their superior performances have been demonstrated experimentally, with good agreement obtained between their simulated and measured *S*-parameters.**

***Index Terms*— Bandpass filter (BPF), fractal, Hilbert resonator, out-of-band rejection, tunable filter.**

I. Introduction

PLANAR varactor-tunable filters with compact structures are very important for the development of multifunctional multiband RF and microwave systems. In the past two decades, their studies have been mainly focused on the frequency tuning function realized by resonant structures [1]–[5], such as combined-line and interdigital resonators. In order to further improve their performances for some integrated compact multiband radio devices, such as home eNodeB [6], both frequency and bandwidth tuning capabilities are required [7]–[18]. By using a stepped-impedance resonator (SIR), a varactor-tunable bandpass filter (BPF) has been realized with a volume of 38 × 38 × 0.8 mm^3 in [7]. Its frequency tuning range is 12.5% at 2.0 GHz, the variation of its 3-dB fractional bandwidth (FBW) is within 3.2%, and the insertion loss is 4–6 dB. Another type of planar varactor-tunable BPF, based on a set of independent electric and magnetic coupling structures, has been presented in [15], in which the filters have been designed with three different FBW variations. In [16], a planar varactor-tunable BPF has been developed with a novel dual-mode resonator, whose its frequency tuning range is 41% from 0.57 to 0.98 GHz.

The above tunable BPFs have frequency and/or bandwidth tuning capabilities. However, it is still very challenging to tune the frequency and bandwidth, suppress the fixed frequency, and miniaturize the volume simultaneously. These three features are very essential for compact advanced multimode and multiband radio devices, including wireless system-on-a-package (SoP) [8], with interference suppression, as indicated in [19] and [20]. In order to find out an appropriate planar structure for the tunable filters with high performance, we resort to the unique Hilbert fractal structure. It has been utilized to build up planar passives [21]–[24], such as antennas, resonators, and high-impedance surfaces, because of its very compact geometry, multiband resonance, and self-similar response. However, to the best of our knowledge, no research has been reported for using the Hilbert fractal structure to design varactor-tunable filters. That is the main motivation of this paper.

In this paper, one type of compact varactor-tunable BPF is proposed using the third-order Hilbert fractal (H_3) resonator. Its frequency tuning is achieved by the loaded varactors, and its out-of-band rejection is accomplished by the external feedlines next to the H_3 resonators. As tuning and rejection are independent of each other, it leads to a simple scheme for both controls, which is very important for multimode and multiband wireless SoP system development. In our design, the H_3 resonator, together with loaded varactors, is carefully analyzed, according to the coupled-line model. Two prototypes have been fabricated and measured to verify our design.

The organization of the rest of this paper is as follows. Section II presents modeling and design of the H_3 resonator and the planar varactor-tunable BPF, and the resonant characteristics of the tunable H_3 resonator are examined numerically. In Section III, the measured and simulated performances are given and analyzed for the two fabricated filter prototypes. Conclusions are drawn in Section IV.

II. Modeling and Design

Fig. 1(a) shows the layout of the proposed tunable BPF, which consists of I/O coupled line sections and two modified

Manuscript received September 26, 2011; revised April 2, 2012; accepted September 12, 2012. Date of publication January 9, 2013; date of current version February 21, 2013. This work was supported by the Major National S&T Programs under Grant 2011ZX03001-003-02, Grant 2011ZX03003-001-03, and Grant 2012ZX03003002, and the National Basic Research Program of China under Grant 2009CB320204. Recommended for publication by Associate Editor L.-T. Hwang upon evaluation of reviewers' comments.

H.-L. Peng, L.-S. Wu, and J. Mao are with the Key Laboratory of the Ministry of Education for Research on Design and EMC of High-Speed Electronic Systems, Shanghai Jiao Tong University, Shanghai 200240, China (e-mail: hl.peng@sjtu.edu.cn; wallish@sjtu.edu.cn; jfmao@sjtu.edu.cn).

W.-Y. Yin is with the Key Laboratory of the Ministry of Education for Research on Design and EMC of High-Speed Electronic Systems, Shanghai Jiao Tong University, Shanghai 200240, China, and also with the Center for Optical and EM Research, State Key Lab of MOI, Zhejiang University, Hangzhou 310058, China (e-mail: wyyin@zju.edu.cn).

D. Huo is with ZTE Corporation, Shanghai 201203, China (e-mail: dhuo@ieee.org).

Color versions of one or more of the figures in this paper are available online at http://ieeexplore.ieee.org.

Digital Object Identifier 10.1109/TCPMT.2012.2222643

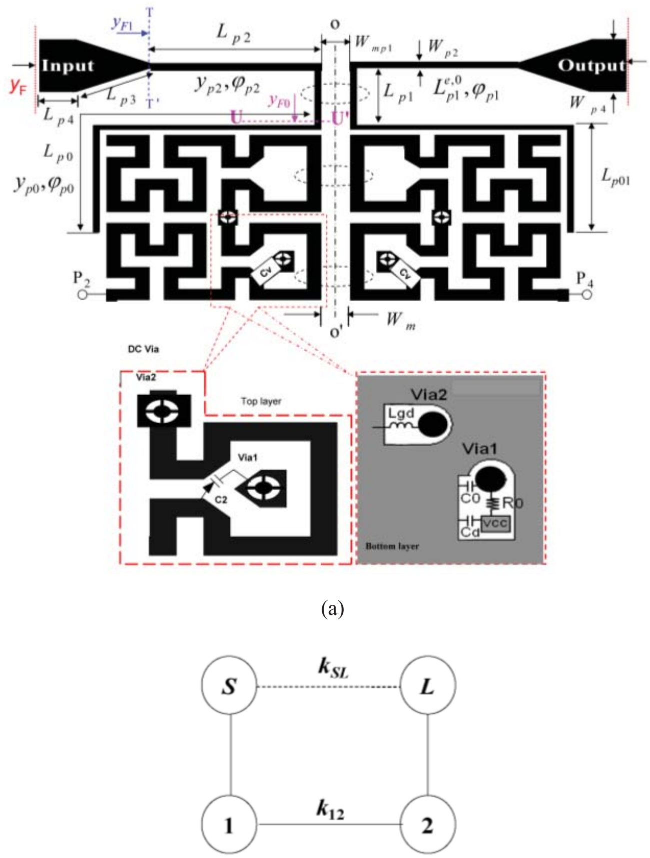

(a)

(b)

Fig. 1. Proposed tunable filter. (a) Layout. (b) Coupling scheme.

H_3 resonators. Each of the resonators is loaded by a varactor C_V. Points indicted by P_2 and P_4 are shorted or opened here.

The coupling scheme of the tunable BPF is shown in Fig. 1(b), where S and L represent its source and load nodes, respectively.

To model and design the filter, both even- and odd-mode input admittances Y_{F1}^{e} and Y_{F1}^{o}, seen from the TT′ plane in Fig. 1(a), is formulated with a magnetic or an electric wall placed at the OO′ plane, respectively

$$Y_{F1}^{e,o} = y_{p2}\frac{A^{e,o}y_{p1}^{e,o} + jB^{e,o}y_{p2}^{\tan}\varphi_{p2}}{B^{e,o}y_{p2} + jA^{e,o}y_{p1}^{e,o}\tan\varphi_{p2}} \tag{1}$$

and

$$A^{e,o} = y_{F0}^{e,o} + jy_{p1}^{e,o}\tan\varphi_{p1} \tag{2}$$

$$B^{e,o} = y_{p1}^{e,o} + jy_{F0}^{e,o}\tan\varphi_{p1} \tag{3}$$

$$y_{F0}^{e,o} = \begin{cases} P_2 \text{ and } P_4 \text{ opened} \\ P_2 \text{ and } P_4 \text{ shorted} \end{cases} \tag{4}$$

where the superscripts e and o represent the even and odd modes, respectively. By looking into the H_3 resonator from the UU′ plane in Fig. 1(a), the input admittances $y_o^{e,o}$ and $y_s^{e,o}$ can be extracted with electromagnetic (EM) simulation. Further, using the circuits approach, the input admittances Y_F^e and Y_F^o at the input port can be obtained from Y_{F1}^e and Y_{F1}^o, respectively.

The overall admittance matrix of the above filter can then be described by

$$\begin{bmatrix} y_{F11} & y_{F12} \\ y_{F21} & y_{F22} \end{bmatrix} = \frac{1}{2}\begin{bmatrix} Y_F^e + Y_F^o & Y_F^e - Y_F^o \\ Y_F^e - Y_F^o & Y_F^e + Y_F^o \end{bmatrix}. \tag{5}$$

In our design, three important issues have to be taken care of, which are as follows.

1) In order to provide a nearly constant filter response shape and bandwidth, the separation between the odd- and even-mode resonant frequencies f_0^o and f_0^e of the H_3 resonator should be kept almost unchanged when changing the capacitance C_V.
2) The derivative of the input susceptance to f_0^o and f_0^e for H_3 resonator's external coupling should be nearly constant so that the filter has a constant bandwidth over the entire frequency tuning range.
3) Rejection at a fixed frequency is realized by the fixed transmission zero at the frequency f_z. Therefore, the input admittances $Y_F^e = Y_F^o$ at f_z is required, as the capacitance C_V changes.

A. H_3 Resonator

With an electric or a magnetic wall inserted at the OO′ plane in Fig. 1(a), two circuits for the odd and even modes with no external coupling are obtained. Their layouts and approximate equivalent circuit models are shown in Fig. 2(a)–(c). For simplicity, we assume that the H_3 resonator consists of transmission lines (TLs), in which the ith TL has electrical length of θ_i. The parasitic and coupling effects of the ith TL within the resonator are considered by reducing the θ_{0i} with $\Delta\theta$, i.e., $\theta_i = \theta_{0i} - \Delta\theta$, where $\Delta\theta$ is about 3.1° in our case and θ_{0i} (i = 1, 2, 3, 4) is the electrical length of the ith TL without parasitic and coupling effects.

In Fig. 2, we add the reference port P_1 to calculate the odd- and even-mode input admittances of the H_3 resonator

$$Y_{in} = \frac{a + (Y_0\tan\theta_3)\,b + [(Z_0\tan\theta_3)\,a + b]\,Y_l}{c + (Y_0\tan\theta_3)\,d + [(Z_0\tan\theta_3)\,c + d]\,Y_l} \tag{6}$$

$$Y_l = j\omega C_V + \begin{cases} +jY_0\tan\theta_4, & P_3 \text{ and } P_4 \text{ opened} \\ -jY_0\cot\theta_4, & P_3 \text{ and } P_4 \text{ shorted} \end{cases} \tag{7}$$

$$a = C_1A_2 + D_1C_2 \tag{8}$$

$$b = C_1B_2 + D_1D_2 \tag{9}$$

$$c = A_1A_2 + B_1C_2 \tag{10}$$

$$d = A_1B_2 + B_1D_2 \tag{11}$$

where $Z_0 = 1/Y_0$, with Y_0 being the characteristic admittances of the transmission lines for the H_3 resonator

$$\begin{bmatrix} A_i & B_i \\ C_i & D_i \end{bmatrix} = \begin{bmatrix} 1 + Z_0Y\tan\theta_i\tan\theta & Z_0\tan\theta_i + Z\tan\theta \\ Y_0\tan\theta_i + Y\tan\theta & \tan\theta(Y_0Z\tan\theta_i + 1) \end{bmatrix}. \tag{12}$$

Equations (6)–(12) can be used to describe both odd- and even-mode characteristics. For the odd mode, we substitute $\theta = \theta^o$ and $Y = Y^o$ into (12), while for the even mode, we substitute $\theta = \theta^e$ and $Y = Y^e$. Y^o and Y^e represent the odd- and even-mode characteristic admittances of the coupled transmission lines, respectively. θ^o and θ^e are their

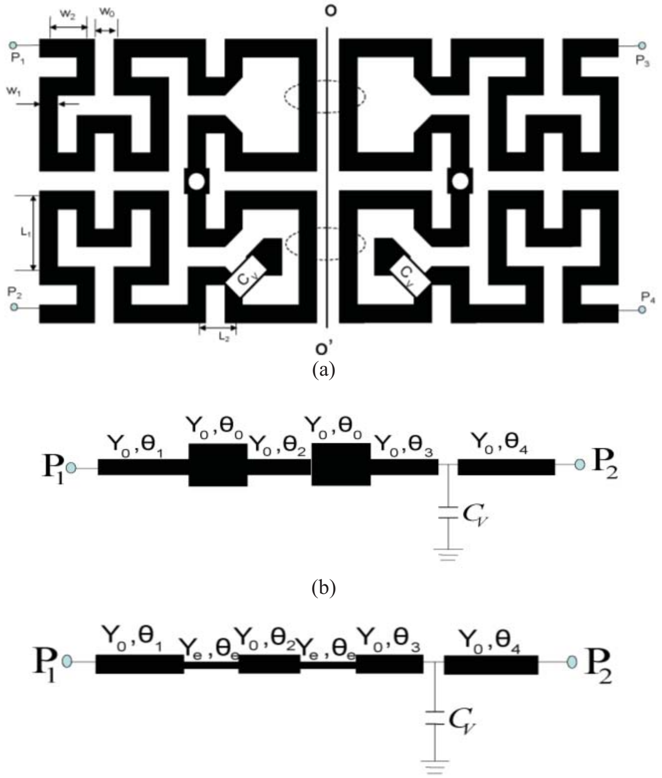

Fig. 2. (a) Layout of the H_3 resonator with an electric and a magnetic wall inserted at the OO′ plane. (b) Its odd- and (c) even-mode equivalent circuits.

corresponding electrical lengths. When $C_V = 0$, the initial length of the single H_3 resonator is determined by its central frequency f_0.

At f_0^o and f_0^e, the following resonant conditions should be satisfied:

$$Im[Y_{ino}(f_0^o)] = 0 \tag{13}$$

$$Im[Y_{ine}(f_0^e)] = 0. \tag{14}$$

Fig. 3 shows the effectiveness of the derived equations to deal with parasitic and coupling effects in the even and odd mode and the variations of the odd- and even-mode resonant frequencies for different values of C_V, with given parameters. It is observed that, for the designed two H_3 resonators, when C_V varies from 0 to 6 [pF], the separation between f_0^o and f_0^e is almost unchanged.

The coupling coefficient k between two H_3 resonators is calculated by

$$k = \frac{\left|(f_0^e)^2 - (f_0^o)^2\right|}{\left|(f_0^e)^2 + (f_0^o)^2\right|} \approx \frac{\left|f_0^e - f_0^o\right|}{f_0}. \tag{15}$$

Fig. 4 shows the coupling coefficient k as a function of the spacing W_m between two H_3 resonators when P_3 and P_4 are opened and $C_V = 0$. This result is extracted from the full-wave EM simulation, and the analytical one is also provided for comparison.

The relative tuning range is defined as the ratio of the frequency tuning range $(f_2 - f_1)$ to the capacitance variation $(C_{V2} - C_{V1})$ when the loading capacitance C_V varies from $C_{V1} = 0.5$ pF to $C_{V2} = 5.5$ pF. Here, f_1 and f_2 are the lowest and highest central frequencies of the tunable H_3 resonator, respectively. To demonstrate how to control the tuning range, the dependence of the tuning frequency on the characteristic admittances Y_0 and electrical lengths of H_3 resonators are investigated. As the odd-mode electrical length $\theta° = 140°$ at 1.9 GHz, the tuning range with Y_0 is calculated for the odd-mode case, which is plotted in Fig. 5(a). In addition, the variation of the tuning range with different $\theta°$ at 1.9 GHz and $Y_0 = 0.009$ is plotted in Fig. 5(b). Based on Fig. 5, the proper linewidth W_1 and the total length of H_3 resonator are obtained for the maximum relative tuning range.

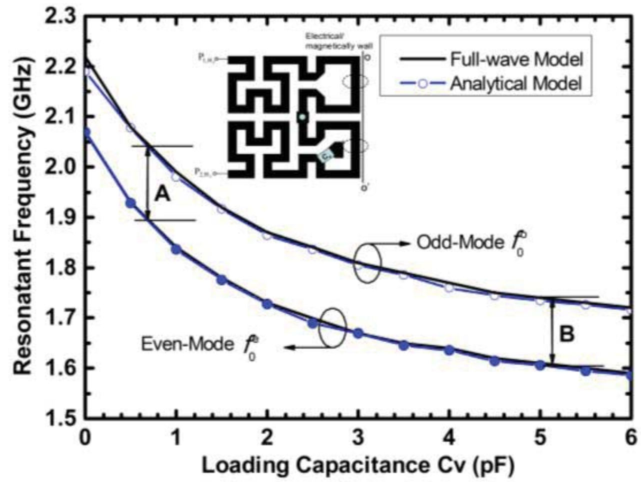

Fig. 3. Resonant frequencies of the odd and even modes as a function of varactor capacitance C_V when P_2 is opened ($W_m = 0.15$, $W_0 = W_1 = 0.5$, $W_2 = 1.02$, $L_1 = 2.05$, and $L_2 = 0.52$ mm).

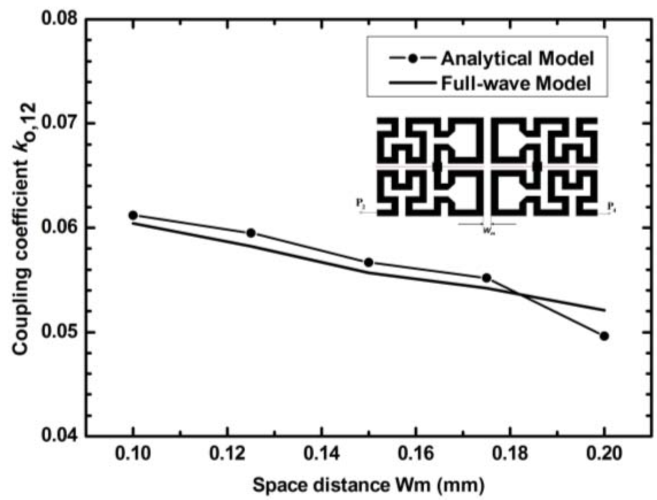

Fig. 4. Coupling coefficient k as a function of the spacing W_m between two H_3 resonators when P_2 and P_4 are opened and $C_V = 0$ pF ($W_m = 0.15$, $W_0 = W_1 = 0.5$, $W_2 = 1.02$, $L_1 = 2.05$, and $L_2 = 0.52$ mm).

B. External Coupling of the H_3 Resonator

Fig. 6 shows the H_3 resonator together with its external coupling structure. The frequency-dependent susceptance slope parameter of Y_{F1}^e and Y_{F1}^o for this structure can be computed from the definition of external quality factor Q_{exe}. For the odd

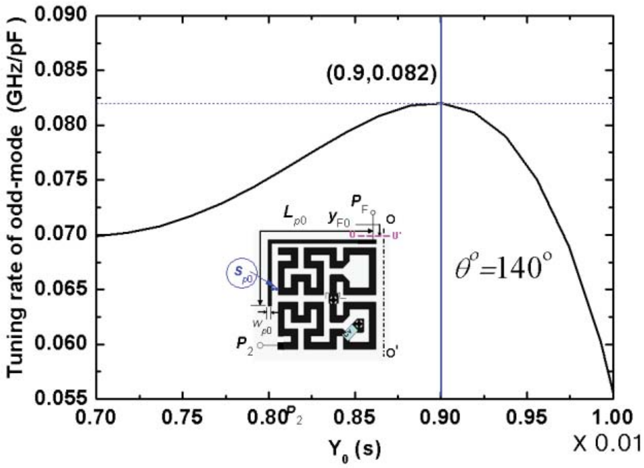

(a)

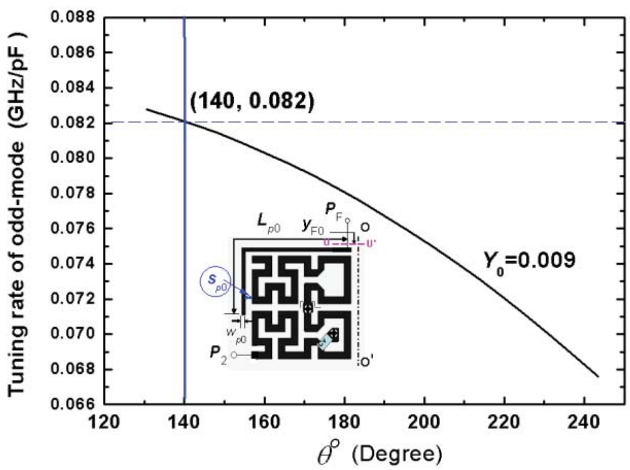

(b)

Fig. 5. Variation of the relative tuning range of the odd mode with (a) Y_0 and (b) $\theta°$, where C_V is varied from 0.5 to 5.5 pF and P_2 shorted (L_{p0} = 12.9, W_{p0} = 0.23, and S_{p0} = 0.25 mm).

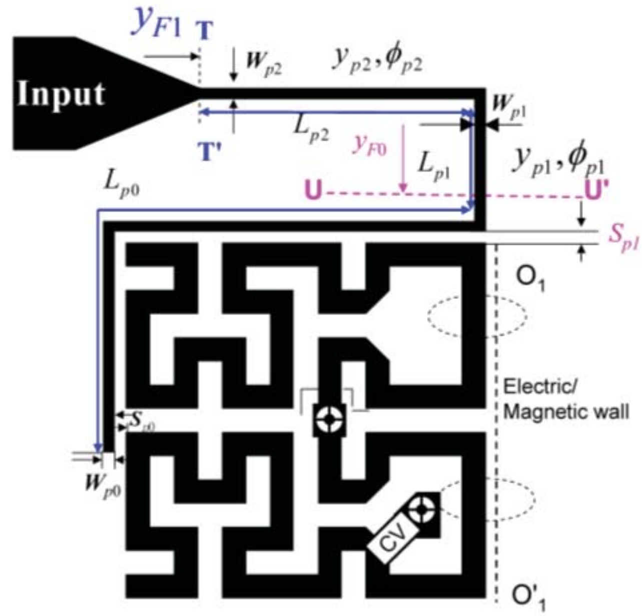

Fig. 6. H_3 resonator together with the external coupling structure.

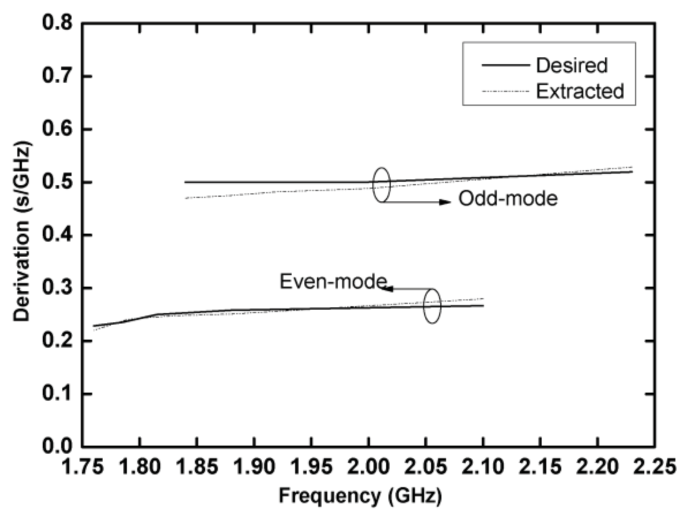

Fig. 7. Derivatives of the input susceptance to the resonated frequency when C_V varies from 0.5 to 5.5 pF and P_2 shorted ($W_m = W_{mp1} = 0.15$, $W_0 = W_1 = 0.5$, $W_2 = 1.02$, $L_1 = 2.05$, $L_2 = 0.52$, $L_{p0} = 12.9$, $W_{p0} = 0.23$, and $S_{p0} = S_{p1} = 0.25$ mm).

mode, we have

$$Q_{ex}^o = \frac{f_0^o}{\Delta f_0^o} = \frac{Z_{\text{port}} f_0^o}{2} \frac{\partial}{\partial f} \text{Im}\left[Y_{F1}^o\left(f_0^o\right)\right] \tag{16}$$

where $Z_{\text{port}} = 50\ \Omega$ is the port impedance, and Q_{ex}^o and Δf_0^o are the external Q-factor and the 3-dB bandwidth of the odd mode, respectively. It can be obtained by

$$\frac{\partial}{\partial f} \text{Im}\left[Y_{F1}^o\left(f_0^o\right)\right] = \frac{2}{Z_{\text{port}} \Delta f_0^o}. \tag{17}$$

Similarly, for the even mode, we have

$$\frac{\partial}{\partial f} \text{Im}\left[Y_{F1}^e\left(f_0^e\right)\right] = \frac{2}{Z_{\text{port}} \Delta f_0^e} \tag{18}$$

where Δf_0^e is the 3-dB bandwidth of the even mode.

It can be seen from (17) and (18) that Δf_0^o and Δf_0^e are unchanged only when the derivative of the input susceptance to f_0^o and f_0^e keeps constant over the entire tuning range. In other words, Im$[Y_{F1}^e]$ and Im$[Y_{F1}^o]$ should be the linear functions of f_0^o and f_0^e when the loading capacitance C_V varies from 0.5 to 5.5 pF.

In order to satisfy the conditions (17) and (18) for all values of C_V at the operated tuning range, appropriate initial values of L_{p0}, S_{p0}, and W_{p0} are required. This can be achieved by properly choosing the geometrical parameters W_{p0}, S_{p0}, and S_{p1} based on EM simulations. In general, for a given L_{p0}, which mainly depends on the transmission zero, a small value of S_{p0} or S_{p1} can provide strong coupling, and the external coupling can be enhanced with W_{p0} decreasing. Fig. 7 gives the desired results obtained from (17) and (18), and the extracted one from the EM simulations.

C. Source-Load Cross Coupling

To improve the filter frequency selectivity, it is important to properly introduce and design the source-load cross coupling.

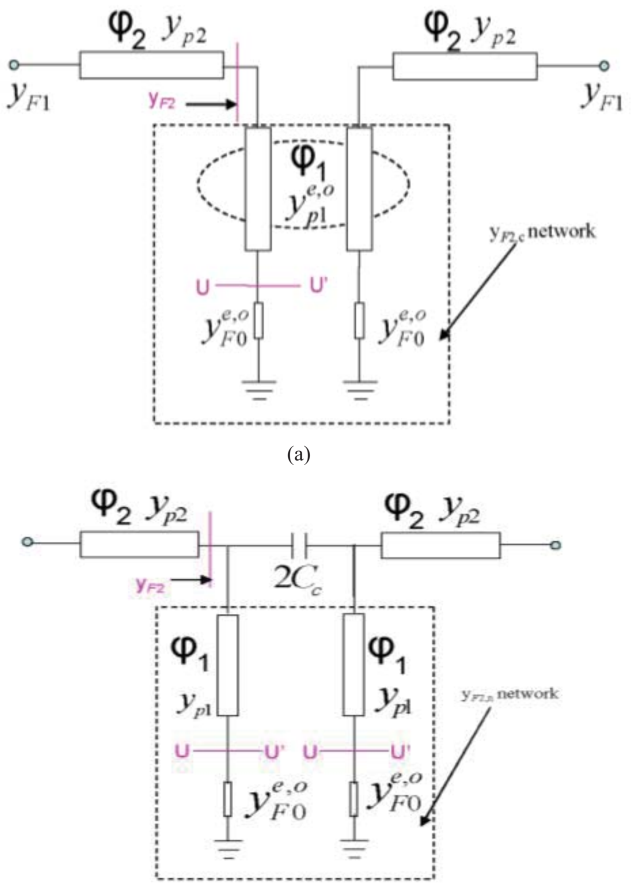

Fig. 8. Source-load cross coupling of the filter. (a) Original circuit model. (b) Simplified circuit model.

Such a design is provided through a section of coupled lines, denoted by L_{p1}, W_{p1}, and W_{mp1} in Fig. 1(a). Because of the small value of L_{p1}, the coupled lines can be approximated by a pair of noncoupled lines, of length L_{p1} and width W_{p1}, with a coupling capacitance C_c in parallel connection, as shown in Fig. 8.

In Fig. 8(b), C_c is extracted by using the parallel network theory, and

$$Y_{F2,c} = \begin{bmatrix} 1 & 1/j\omega C_c \\ 0 & 1 \end{bmatrix} + Y_{F2,n} \tag{19}$$

where

$$Y_{F2,c} = \frac{1}{2}\begin{bmatrix} Y_{F2,c}^{e} + Y_{F2,c}^{o} & Y_{F2,c}^{e} - Y_{F2,c}^{o} \\ Y_{F2,c}^{e} - Y_{F2,c}^{o} & Y_{F2,c}^{e} + Y_{F2,c}^{o} \end{bmatrix} \tag{20}$$

$$Y_{F2,n} = \frac{1}{2}\begin{bmatrix} Y_{F2,n}^{e} + Y_{F2,n}^{o} & Y_{F2,n}^{e} - Y_{F2,n}^{o} \\ Y_{F2,n}^{e} - Y_{F2,n}^{o} & Y_{F2,n}^{e} + Y_{F2,n}^{o} \end{bmatrix}. \tag{21}$$

For the coupled lines L_{p1}, the input admittances of the even and odd modes $Y_{F2,c}^{e,o}$ are calculated by

$$Y_{F2,c}^{e,o} = y_p \frac{y_{F0}^{e} + j y_{p1}^{e,o} \tan\phi_1}{y_{p1}^{e,o} + j y_{F0}^{e} \tan\phi_1}. \tag{22}$$

TABLE I

DIMENSIONS OF THE TUNABLE FILTER (mm)

W_0	W_1	W_2	L_1	L_2	W_m	W_{p0}	L_{p0}	S_{p0}
0.5	0.5	1.02	2.05	0.52	0.15	0.23	12.9	0.25
W_{p1}	W_{p2}	L_{p0}	L_{p1}	L_{p2}	L_{p3}	L_{p4}	S_{p1}	W_{p4}
0.3	0.3	12.9	2.54	5.87	2.84	3.66	0.25	2.44

$W_m = W_{mp1}$.

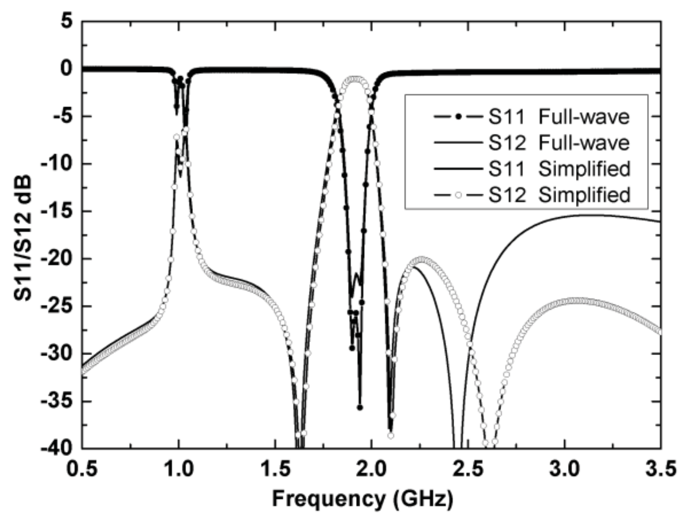

Fig. 9. S-parameters of the filter obtained with EM simulations and simplified circuit model with P_3 and P_4 shorted ($W_m = W_{mp1} = 0.15$, $W_0 = W_1 = 0.5$, $W_2 = 1.02$, $L_1 = 2.05$, $L_2 = 0.52$, $L_{p0} = 12.9$, $W_{p0} = 0.23$, and $S_{p0} = S_{p1} = 0.25$ mm).

Similarly, for a noncoupled line, the input admittance $Y_{F2,n}^{e,o}$ is

$$Y_{F2,n}^{e,o} = y_p \frac{y_{F0}^{e,o} + j y_{p1} \tan\phi_1}{y_{p1} + j y_{F0}^{e,o} \tan\phi_1}. \tag{23}$$

When the parameters shown in Table I and (19) are used, the value of $C_c = 0.057$ pF is obtained. To validate our simplified model, full-wave simulations are carried out, with the results plotted in Fig. 9.

D. Fixed Out-of-Band Rejection

At the fixed out-of-band rejection frequency f_z, which is far from the tuning range of the resonator, the EM coupling between the feed line L_{p0} and the H_3 resonator is very weak, due to their frequency detuning. Therefore, for the given width, W_{p0} and W_{p1} of the microstrip line, the filter's response characteristics at f_z are mainly dominated by its end-opened line length L_p, made of $L_p = L_{p0} + L_{p1}$ (see Fig. 6). In addition, this frequency detuning leads to the characteristics of H_3 resonator with loaded varactors to be almost independent of the filter performance at f_z. This means that the frequency tuning is independent of its out-of-band rejection. This feature of the filter can be used to design the tunable filter with out-of-band fixed rejections as in the following approaches.

Once ϕ_{p1} (or L_{p1}) and W_{p1} are determined by the needed source and load coupling first (frequency tuning), the ϕ_{p0}

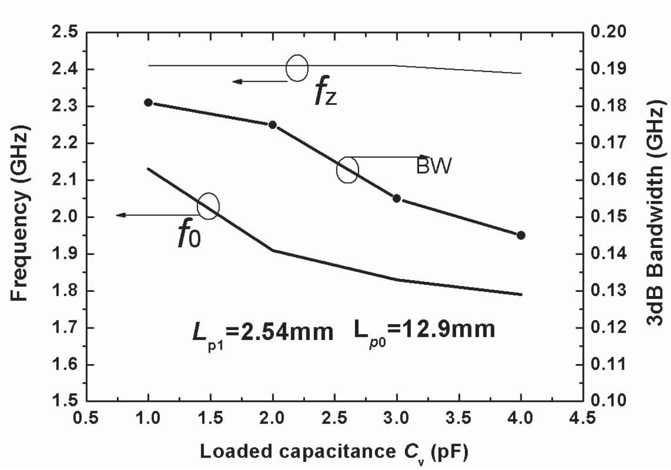

(a)

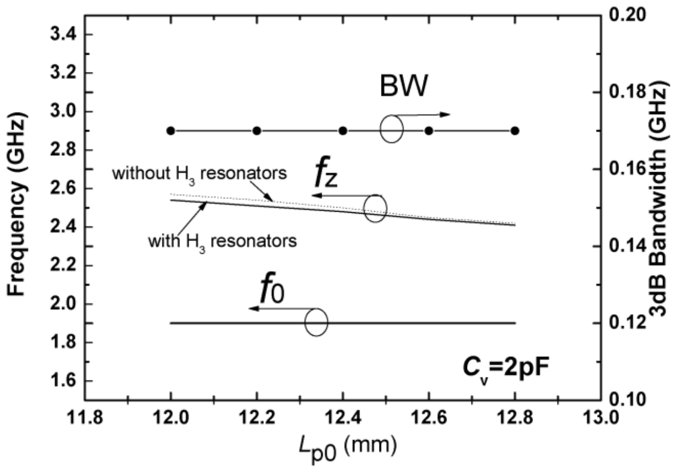

(b)

Fig. 10. Central frequency f_0 and rejection frequency f_z of the filter as functions of (a) capacitance C_V and (b) length $L_{p0} = 7.92 + L_{p01}$ ($W_m = W_{mp1} = 0.15$, $W_0 = W_1 = 0.5$, $W_2 = 1.02$, $L_1 = 2.05$, $L_2 = 0.52$, $W_{p0} = 0.23$, and $S_{p0} = S_{p1} = 0.25$ mm).

(or L_{p0}) can then be determined by using transmission zero condition of the end-opened lines L_p, $y^e_{in}(f_z) = y^o_{in}(f_z)$ without H_3 resonators existence

$$y^e_{p1}\tan(\phi^e_{p0} + \phi_{p1}) = y^o_{p1}\tan(\phi^o_{p0} + \phi_{p1}) \tag{24}$$

and

$$\phi^{e,o}_{p0} = \tan^{-1}\left(\frac{y_{p0}\tan\phi_{p0}}{y^{e,o}_{p1}}\right) \tag{25}$$

where y_{p0}, ϕ_{p0}, y^e_{p1}, y^o_{p1}, and ϕ_{p1} are as shown in Fig. 1(a).

Corresponding to $L_{p0} = 12.9$ mm and $L_{p1} = 2.54$ mm when P_2 and P_4 ports are shorted, Fig. 10(a) shows the central frequency f_0 and f_z against the capacitance C_V varying from 1.0 to 5.0 pF. Fig. 10(b) shows the variations of f_0 and f_z for different values of L_{p01} [see Fig. 1(a)] when $C_V = 2$ pF. The former shows that the f_z is nearly a constant for the given L_{p0} and L_{p1} over the tuning range. The latter shows that the longer the length L_{p01}, the smaller the f_z obtained.

Our design procedure of the tunable filter is summarized as follows.

TABLE II

Parameters for Filter Prototypes A and B

Samples	A	B
Size (mm^3)	20.0 × 13.0 × 1.0	20.0 × 13.0 × 1.0
Frequency tunability	13%	7.4%
Insertion loss (dB)	1.7	4.5
3-dB FBW	9.3%	11.3%
Central frequency (GHz)	1.71	1.95
Rejection (dB)	–35@2.4 GHz	–28@2.48 GHz

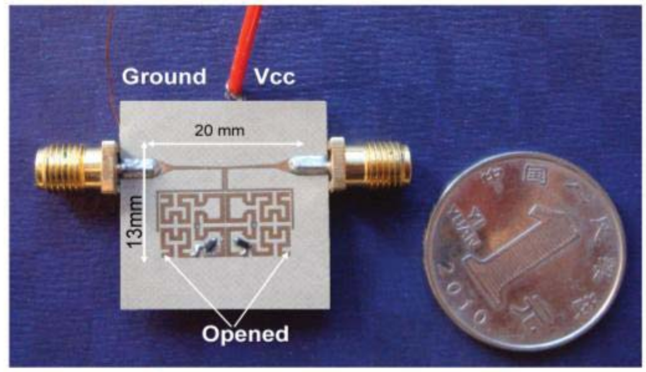

(a)

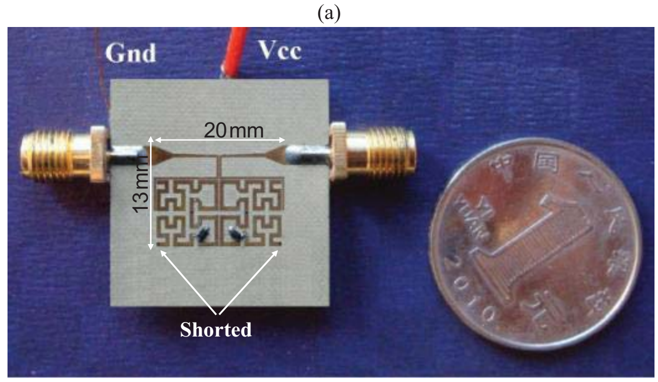

(b)

Fig. 11. Photographs of the filter prototypes. (a) Filter A. (b) Filter B.

1) According to the upper limit of the given frequency tuning range and the given minimum value of C_V, the initial parameters of two H_3 resonators (W_0, W_1, W_2, L_1, and L_2) are achieved.
2) As the BPF characteristics are given, the coupling coefficients k_{12} between two H_3 resonators, and k_{SL} between the source and the load, can be synthesized based on the theory of elliptical filters with double poles.
3) According to the desired value of k_{12}, the spacing W_m between the two H_3 resonators is determined.
4) Based on the desired value of k_{SL}, the parameters $y^{e,o}_{p1}$ and ϕ_{p1}, i.e., L_{p1}, W_{p1}, and W_{mp1}, can be determined. Furthermore, the geometrical parameters W_{p0}, S_{p0}, S_{p1}, and the initial L_{p0} are obtained by minimizing the derivatives of both even- and odd-mode input susceptances.
5) The length L_{p1} of the external lines is finally determined by the required out-of-band rejection at f_z over the entire tuning range.

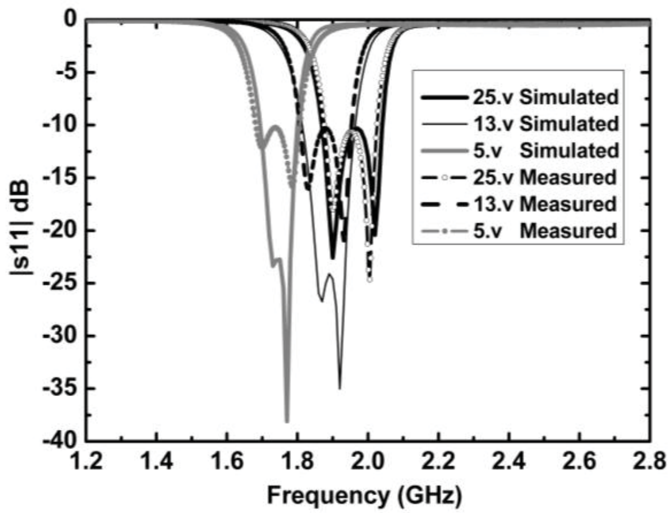

(a)

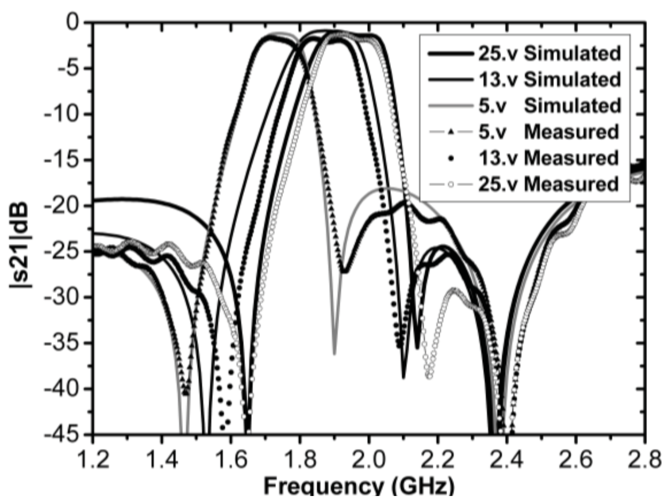

(b)

Fig. 12. Simulated and measured S-parameters of filter A. (a) Reflection coefficients. (b) Transmission coefficients.

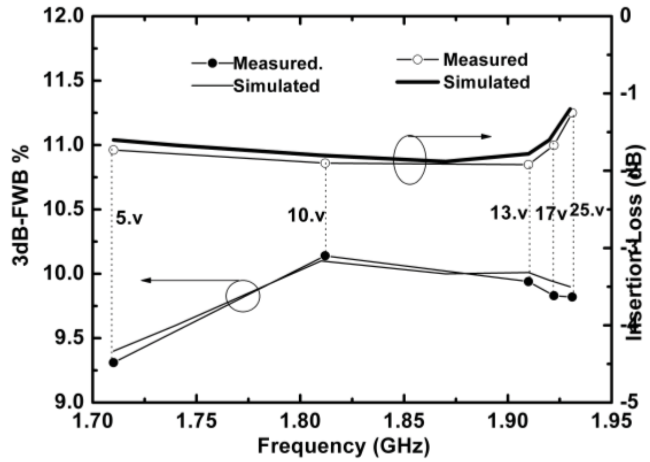

Fig. 13. Measured insertion loss, 3-dB bandwidth, and central frequency of filter A with different bias voltages.

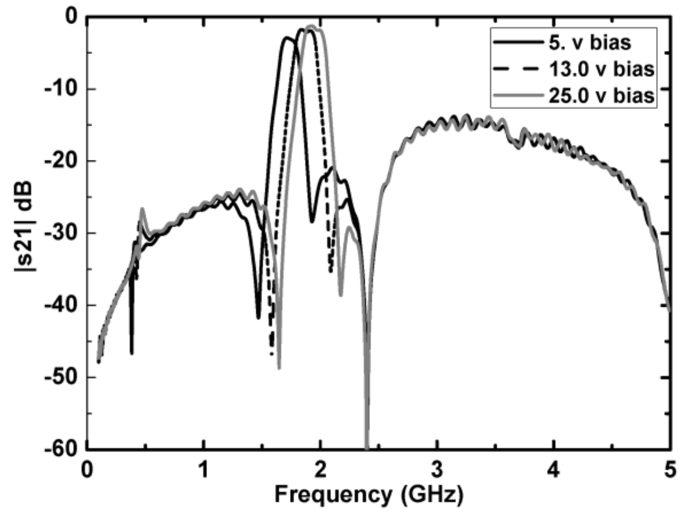

Fig. 14. Measured harmonic response of filter A.

III. Results and Discussion

To validate our design, two filter prototypes, denoted A and B, are fabricated on a Taconic TSM-30 substrate, which has the relative permittivity of 3.0 and the thickness of 1.016 mm. Their dimensions and main performance parameters are listed in Tables I and II, respectively, and their photographs are shown in Fig. 11.

In their realizations, the RF circuits, including two H_3 resonators, two external coupled feedlines, and two loaded Infineon BB857 varactors [26], are located on the top PCB layer. The d.c. bias circuits shown in Fig. 1(a), consisting of two AVX chip capacitors $C_0 = 15.4$ and $C_d = 30$ pF, a resistor $R_0 = 1.0$ MΩ, and an AVX chip inductor $L_{gd} = 39$ nH, are on its bottom layer. Here, C_0 is series-connected with the varactor capacitance C_{V0}, C_d is a decoupling capacitor, R_0 isolates the d.c. from the RF signal, and L_{gd} is used as the RF choke. Four metallic via-holes, each with a diameter of 0.25 mm, are utilized to connect both RF and d.c. bias circuits.

A. Open-Ended Tunable Filter A

As shown in Fig. 11(a), filter A has an overall volume of $25.0 \times 17.0 \times 1.0$ mm^3 with P_2 and P_4 open ended. Fig. 12 shows its simulated and measured S-parameters. With the bias voltage of 5 V, the central frequency is about 1.71 GHz, and the 3-dB FBW is 9.3%, with an in-band insertion loss of 1.7 dB, as shown in Fig. 13. When the bias voltage is increased to 25 V, the central frequency moves to 1.93 GHz, and the 3-dB FBW is 9.9%, with an insertion loss of 1.24 dB. In Fig. 13, the measurement shows an almost constant FBW, and the variation is within 0.6%, i.e., the frequency of filter A can be tuned with a nearly constant FBW. The measured in-band return loss is always better than 10 dB over the entire tuning range. At both the lower and upper stop bands, the out-of-band rejections are better than 19 dB. The variation of insertion loss, when the central frequency moves from 1.71 to 1.93 GHz, is smaller than 0.8 dB.

Fig. 14 shows the measured harmonic response of filter A. It is observed that the bias voltage has little impact on its frequency responses in the lower stopband from 0.1 to 1.3 GHz

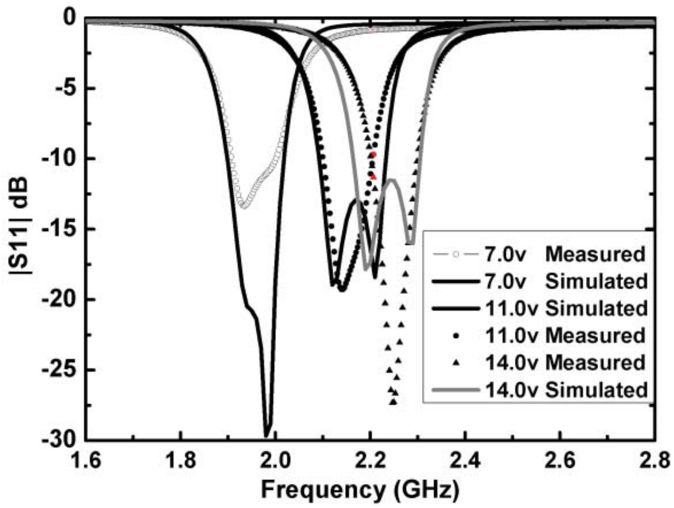

(a)

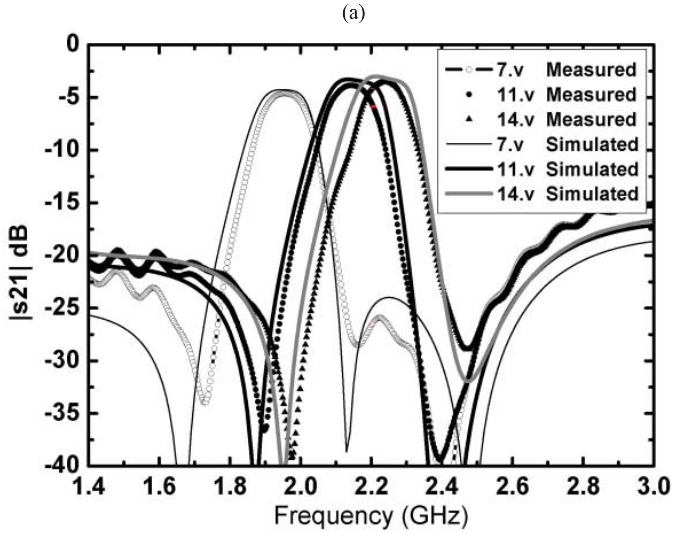

(b)

Fig. 15. Simulated and measured *S*-parameters of filter B. (a) Reflection coefficients. (b) Transmission coefficients.

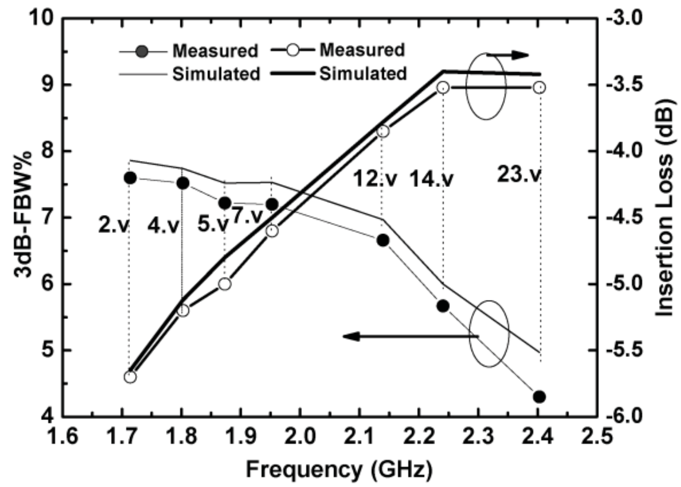

Fig. 16. Measured insertion loss, 3-dB bandwidth, and central frequency of filter B for different bias voltages.

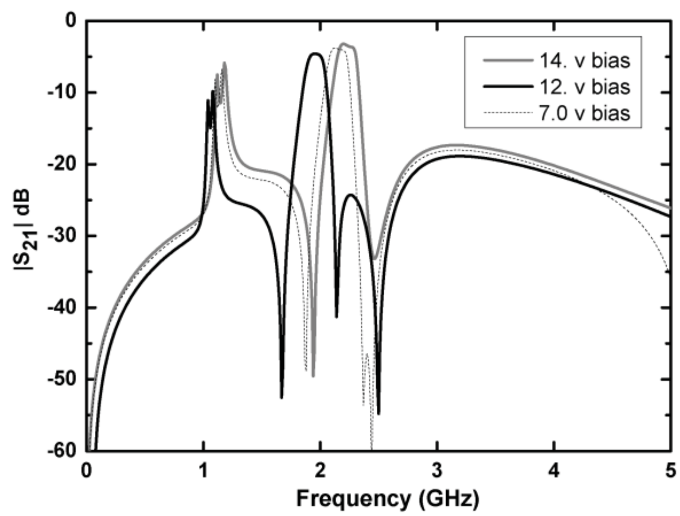

Fig. 17. Measured harmonic response of filter B.

and the upper one from 2.5 to 5.0 GHz. Their rejections are lower than −25.0 and −16.0 dB. There is a fixed transmission zero at 2.4 GHz, independent of the varactor capacitance. Such a property is useful for interference suppression.

B. Short-Ended Tunable Filter B

As shown in Fig. 11(b), filter B is has the same volume as filter A. P_2 and P_4 are short-ended in this case. Fig. 15 shows good agreement between its measured and simulated *S*-parameters. Its frequency tuning range is from 1.98 to 2.4 GHz; the measured in-band return and insertion losses are larger than 12 and 4.5 dB over the entire operating bandwidth, respectively. The insertion loss of filter B is larger than that of filters A, mainly due to the reduction of its FBW.

As shown in Fig. 16, when the bias voltage varies from 2 to 14 V, the central frequency of filter B is increased from 1.71 to 2.25 GHz, the 3-dB FBW is decreased from 7.6% to 5.7%, and the insertion loss is decreased from 5.7 to 3.5 dB. In other words, the FBW of filter B is decreased with its tuning frequency increasing.

Fig. 17 shows the measured harmonic response of filter B with the bias voltage varying from 7 to 14 V. A parasitic response arises around 1.1 GHz, with the level about −10 dB. It is because, at the frequency around 1 GHz, the H_3 resonator of filter B is operated in its nearly $1/4\lambda_g$ resonant mode, which leads to the spurious passband. At around 2 GHz, the resonator is operated in its nearly $3/4\lambda_g$ resonant mode.

The ratio of their resonant frequencies deviates from 3 because of the capacitive loading effect. Similar to filter A, there is also little impact of bias voltage on the frequency responses of filter B in the lower stop band from 0.1 to 1.0 GHz and the upper one from 2.5 to 5.0 GHz. The harmonic responses in the lower and upper stop bands are lower than −25.0 and −16.0 dB, respectively. At about 2.48 GHz, there is also a fixed transmission zero. The performances of filter A and B compared with the previously published ones are shown in Table III. It is observed that our tunable BPFs are very compact in size and also have a fixed out-of-band rejection. These features are very

TABLE III

DETAILED COMPARISON OF THE PROPOSED FILTERS WITH PREVIOUSLY PUBLISHED FILTERS

Ref.	Frequency Tuning Range (GHz)	Bandwidth Tuning Range	IL (dB)	Fixed Out-of-Band Reject	Normalized Area (λ_0^2)	Feature
[2]	1.00–1.33	15%	$\leq$3.0	No	0.04	1
[7]	1.85–2.15	3.2%	$\leq$6.0	No	0.17	1
[10]	2.10–2.70	0.3%	$\leq$5.0	No	0.67	2
[13]	0.47–0.86	33%	$\leq$4.0	No	0.032	*
[15]	0.85–1.40	5.4%	$\leq$2.9	No	0.036	2
	0.91–1.34	5.2–2.9%	$\leq$2.9	No	0.036	1
	0.86–1.41	4.3–6.5%	$\leq$3.5	No	0.036	3
[16]	0.60–1.07	14–8.2%	$\leq$1.8	No	*	3
	0.57–0.98	16–9.2%	$\leq$2.2	No	*	3
[17]	1.40–2.00	9%	$\leq$4.0	No	0.033	*
Filter A	1.71–1.93	**9.3–9.9%**	$\leq$1.7	**–35 dB**	**0.021**	**2**
Filter B	1.92–2.25	7.6–5.7%	$\leq$4.1	**–30 dB**	**0.021**	4

1: Constant BW. 2: Constant FBW. 3: Increased FBW. 4: Decreased FWB. * No data.

useful for multimode and multiband wireless SoP system applications.

IV. CONCLUSION

In this paper, a new compact planar tunable filter was proposed with tunable frequency and fixed out-of-band rejection. The filter design is based on the Hilbert fractal structures loaded with varactors. The frequency tuning and its out-of-band rejection are independent of each other, which makes its operation simple. The circuit model and design procedure of the tunable filter were presented. Two filter prototypes were realized to validate our design. Filter A had a nearly constant FBW, while filter B had a decreasing FBW with increasing bias voltage of the varactor. Both of them had fixed out-of-band transmission zero, which could be utilized for interference suppression. Good agreement was obtained between the measured and simulated results for each filter prototype, and their frequency tuning and rejection capabilities were demonstrated.

REFERENCES

[1] I. C. Hunter and J. D. Rhodes, "Electronically tunable microwave bandpass filters," *IEEE Trans. Microw. Theory Tech.*, vol. 30, no. 9, pp. 1354–1360, Sep. 1982.

[2] A. R. Brown and G. M. Rebeiz, "A varactor-tuned RF filter," *IEEE Trans. Microw. Theory Tech.*, vol. 48, no. 7, pp. 1157–1160, Jul. 2000.

[3] L. Dussopt and G. M. Rebeiz, "Intermodulation distortion and power handling in RF MEMS switches, varactors, and tunable filters," *IEEE Trans. Microw. Theory Tech.*, vol. 51, no. 2, pp. 462–467, Feb. 2003.

[4] J. Nath, D. Ghosh, J. P. Maria, A. I. Kingon, W. Fathelbab, P. D. Franzon, and M. B. Steer, "An electronically tunable microstrip bandpass filter using thin-film barium-strontium-titanate (BST) varactors," *IEEE Trans. Microw. Theory Tech.*, vol. 53, no. 9, pp. 2707–2712, Sep. 2005.

[5] G. L. Matthaei, L. Young, and E. M. T. Jones, *Microwave Filters, Impedance-Matching Networks, and Coupling Structures*. Norwood, MA: Artech House, 1980.

[6] *3GPP Specification Series*. (2012) [Online]. Available: http://www.3gpp.org/ftp/Specs/html-info/34-series.htm

[7] B.-W. Kim and S.-W. Yun, "Varactor-tuned combline bandpass filter using step-impedance microstrip lines," *IEEE Trans. Microw. Theory Tech.*, vol. 52, no. 4, pp. 1279–1283, Apr. 2004.

[8] C. Lugo and J. Papapolymerou, "Electronic switchable bandpass filter using PIN diodes for wireless low cost system-on-a-package applications," *IEE Proc. Microw. Antennas Propag.*, vol. 151, no. 6, pp. 497–502, Dec. 2004.

[9] P. W. Wong and I. C. Hunter, "A new class of low-loss high-linearity electronically reconfigurable microwave filters," *IEEE Trans. Microw. Theory Tech.*, vol. 56, no. 8, pp. 1945–1953, Aug. 2008.

[10] J. Lee, and K. Sarabandi, "An analytic design method for microstrip tunable filters," *IEEE Trans. Microw. Theory Tech.*, vol. 56, no. 7, pp. 1699–1706, Jul. 2008.

[11] M. Koochakzadeh and A. A. Tamijani, "Tunable filters with nonuniform microstrip coupled lines," *IEEE Microw. Wireless Compon. Lett.*, vol. 18, no. 5, pp. 314–316, May 2008.

[12] J.-S. Hong, "Reconfigurable planar filters," *IEEE Microw. Mag.*, vol. 10, no. 9, pp. 73–83, Oct. 2009.

[13] M. S. Renedo, R. G. Garcia, J. I. Alonso, and C. B. Rodriguez, "Tunable combline filter with continuous control of center frequency and bandwidth," *IEEE Trans. Microw. Theory Tech.*, vol. 53, no. 1, pp. 191–199, Jan. 2005.

[14] S. J. Park, K. V. Caekenberghe, and G. M. Rebeiz, "A miniature 2.1 GHz low loss microstrip filter with independent electric and magnetic coupling," *IEEE Microw. Wireless Compon. Lett.*, vol. 14, no. 10, pp. 496–498, Oct. 2004.

[15] S. J. Park and G. M. Rebeiz, "Low-loss two-pole tunable filters with three different predefined bandwidth characteristics," *IEEE Trans. Microw. Theory Tech.*, vol. 56, no. 5, pp. 1137–1148, May 2008.

[16] W.-X. Tang and J.-S. Hong, "Varactor-tuned dual-mode bandpass filters," *IEEE Trans. Microw. Theory Tech.*, vol. 58, no. 8, pp. 2213–2219, Aug. 2010.

[17] J. Long, C.-Z. Li, W.-Z. Cui, J.-T. Tao, H. Fu, and L.-X. Ran, "A tunable microstrip bandpass filter with two independently adjustable transmission zeros," *IEEE Microw. Wireless Compon. Lett.*, vol. 21, no. 2, pp. 74–76, Feb. 2011.

[18] J.-S. Hong and M. J. Lancaster, *Microstrip Filters for RF/Microwave Applications*. New York: Wiley, 2001.

[19] *3GPP Specification Series*. (2012) [Online]. Available: http://www.3gpp.org/ftp/Specs/html-info/34-series.htm

[20] R. Arkiszewski, "Multi-mode, multi-band RF front end challenges and solution," in *Proc. IEEE RFIC Symp. Workshop*, May 2010, pp. 1–38.

[21] J. Zhou, A. Hoorfar, and N. Engheta, "Bandwidth, cross polarization, and feed-point characteristics of matched Hilbert antennas," *IEEE Antennas Wireless Propag. Lett.*, vol. 2, no. 1, pp. 2–5, Jan. 2003.

[22] J. McVay, A. Hoorfar, and N. Engheta, "Thin absorbers using space-filling curve high impedance surfaces," *IEEE Microw. Wireless Compon. Lett.*, vol. 14, no. 3, pp. 22–25, Mar. 2004.

[23] J. McVay, N. Engheta, and A. Hoorfar, "High impedance metamaterial surfaces using Hilbert-curve inclusions," *IEEE Microw. Wireless Compon. Lett.*, vol. 14, no. 3, pp. 130–132, Mar. 2004.

[24] N. Jankovic, V. Radonic, and V. C. Bengin, "Novel bandpass filters based on grounded Hilbert fractal resonators," in *Proc. 3rd Int. Congr. Adv. Electromagn. Mater. Microw. Opt.*, Aug. 2009, pp. 728–730.

[25] *BB857 Datasheet*, Infineon, Neubiberg, Germany, Jul. 2001.

Hong-Li Peng (M'10) was born in 1966. He received the B.S., M.S., and Ph.D. degrees in electromagnetic fields and microwave techniques from Xidian University, Xi'an, China, in 1988, 1991, and 2005, respectively.

He was a Senior Researcher and the Project Leader with the Department of Wireless Telemeter Engineering, National Telemeter Center, Xi'an, from 1994 to 1999, where he was involved in the development and system design of a conformal antenna. In 1999, he joined the ZTE Corporation, Shanghai, China, as a Scientific Researcher and the Project Leader, where he contributed to 11 essential patents. Since 2008, he has been an Associate Professor of electromagnetic fields and microwave techniques with the School of Electronic Information and Electrical Engineering, Shanghai Jiao Tong University, Shanghai. He has authored or co-authored more than 45 technical papers and holds over 25 patents. He has authored a book on MIMO indoor channel modeling. His current research interests include tunable radio frequency and microwave passive circuits research, reconfigurable compact antennas and array analysis and design, and spatial wireless channel modeling.

Dr. Peng was a recipient of the Standardization Award of China in 2005 and 2006, and the Science and Technology Promotion Award of the first class from the local Shanghai Government of China in 2011. He was a Session Co-Chair of the 2011 IEEE Electrical Design of Advanced Packaging and Systems Symposium (EDAPS'2011), technically sponsored by the IEEE CPMT Committee, and a Program Committee Co-Chair of the 2012 IEEE International Conference on Cloud Computing and Intelligent Systems (2nd IEEE CCIS2012).

Lin-Sheng Wu (S'09–M'10) was born in 1981. He received the B.S. degree in electronic and information engineering and the M.S. and Ph.D. degrees in electromagnetic fields and microwave technologies from Shanghai Jiao Tong University (SJTU), Shanghai, China, in 2003, 2006, and 2010, respectively.

He was a Research Fellow with the Department of Electrical and Computer Engineering, National University of Singapore, Singapore, in 2010. From 2010 to 2012, he was a Post-Doctoral Researcher with SJTU, where he is currently a Lecturer with the Key Laboratory of the Ministry of Education of Design and Electromagnetic Compatibility of High Speed Electronic Systems. He has authored or co-authored more than 50 technical papers. His current research interests include novel techniques for microwave integration, passive components, and carbon nanoelectronics.

Dr. Wu was a Session Co-Chair of the Asia-Pacific Microwave Conference and the IEEE Electrical Design of Advanced Packaging and Systems Symposium in 2011. He is a reviewer of several international journals, including three IEEE TRANSACTIONS and LETTERS.

Wen-Yan Yin (M'92–SM'98) received the M.Sc. degree in electromagnetic fields and microwave techniques from Xidian University, Xi'an, China, and the Ph.D. degree in electrical engineering from Xi'an Jiao Tong University, Xi'an, in 1989 and 1994, respectively.

He was an Associate Professor with the Department of Electronic Engineering, Northwestern Polytechnic University, Xi'an, from 1993 to 1996. From 1996 to 1998, he was a Research Fellow with the Department of Electrical Engineering, Duisburg University, Duisburg, Germany, granted by the Alexander von Humboldt-Stiftung Foundation, Bonn, Germany. In 1998, he joined as a Research Fellow the Monolithic Microwave Integrated Circuit Modeling and Package Laboratory, Department of Electrical Engineering, National University of Singapore, Singapore, where he then joined the Temasek Laboratories as a Research Scientist and the Project Leader and was involved in research on high-power microwave and ultrawide-band electromagnetic compatibility (EMC)/electromagnetic interference in 2002. Since 2005, he has been a Professor of electromagnetic fields and microwave techniques with the School of Electronic Information and Electrical Engineering, Shanghai Jiao Tong University, Shanghai, China, where he is the Director and the current adjunct Ph.D. He is a Candidate Supervisor with the Center for Microwave and RF Technologies. Since 2009, he has been with the Center for Optical and Electromagnetic Research, National State Key Laboratory of Modern Optical Instrumentation, Zhejiang University, Hangzhou, China, as a Qiu Shi Chair Professor. He has been the lead author of more than 190 co-authored international journal articles (more than 70 IEEE papers), one international book, and 17 book chapters. His current research interests include passive and active radio frequency and millimeter-wave devices and circuit modeling, ultra wideband interconnects and signal integrity, nanoelectronics, EMC, and electromagnetic protection of communication platforms, computational multiphysics, and its applications.

Dr. Yin was a recipient of the Science and Technology Promotion Award of the first class from the local Shanghai Government of China in 2005 and the National Technology Invention Award of the second class from the Chinese Government in 2008. He has been the Guest Editor of the IEEE TRANSACTIONS ON COMPONENTS, PACKAGING AND MANUFACTURING TECHNOLOGY since 2011 and an Associate Editor of the *International Journal of Electronic Networks, Devices and Fields* since 2011. He was the Technical Chair of EDAPS'2006, an IEEE EMC Society Distinguished Lecturer from 2011 to 2012, and the General Co-Chair of the 2011 IEEE Electrical Design of Advanced Packaging and Systems Symposium (EDAPS'2011). He is an Editorial Board Member of the *International Journal of RF and Microwave CAE*, JEMWA, and PIER. He is a Reviewer of many international journals, including eight IEEE TRANSACTIONS and LETTERS.

David Huo (M'92) received the Dipl.Ing., Dipl.Math., and Dr.Ing. degrees from the University of Kassel, Kassel, Germany, in 1992.

He was a Scientific Researcher with Mannesmann Corporation, Düsseldorf, Germany, from 1992 to 1997, and with Lucent Technologies, Nurnberg, Germany, from 1997 to 2007, respectively, where he was involved in research in the telecommunications industry, including network design, wireless access, computer simulation, channel coding, and applied statistics. Since 2008, he has been with ZTE R&D, overseeing research and standardization. His current research interests include optical communication, network architectures, information theory, wave propagation, applied mathematics, and theoretical physics.

Dr. Huo is a member of AIP and MAA.

Junfa Mao (M'92–SM'98–F'12) was born in 1965. He received the B.S. degree in radiation physics from the University of Science and Technology of National Defense, Hefei, China, the M.S. degree in experimental nuclear physics form the Shanghai Institute of Nuclear Research, Shanghai, China, and the Ph.D. degree in electronic engineering from Shanghai Jiao Tong University, Shanghai, in 1985, 1988, and 1992, respectively.

He has been a Faculty Member with Shanghai Jiao Tong University, Shanghai, since 1992, where he is currently a Chair Professor and the Executive Dean of the School of Electronic, Information and Electrical Engineering. He was a Visiting Scholar with the Chinese University of Hong Kong, Hong Kong, from 1994 to 1995, and a Post-Doctoral Researcher with the University of California, Berkeley, from 1995 to 1996. He has authored or co-authored more than 190 journal papers (including 70 IEEE journal papers) and 120 international conference papers. His current research interests include interconnect and package problems of integrated circuits and systems, and analysis and design of microwave circuits.

Dr. Mao was the recipient of the National Natural Science Award of China in 2004, the Best Paper Award of the 2008 Symposium of APEMC in conjunction with the 19th International Symposium of Zurich EMC, and the National Technology Invention Award of China in 2008. He is the Chief Scientist of The National Basic Research Program (973 Program) of China, the Project Leader of the National Science Foundation for Creative Research Groups of China, a Cheung Kong Scholar of the Ministry of Education, China, and an Associate Director of the Microwave Society of China Institute of Electronics. He was the 2007–2009 Chair of the IEEE Shanghai Section and the 2009-2011 Chair of the IEEE MTT Shanghai Chapter.